Efficient three-photon excitation of quasi-one-dimensional strontium Rydberg atoms with $n \sim 300$

S. Ye,[1] X. Zhang,[1] F. B. Dunning,[1] S. Yoshida,[2] M. Hiller,[2,3] and J. Burgdörfer[2]

[1]*Department of Physics and Astronomy and the Rice Quantum Institute, Rice University, Houston, Texas 77005-1892, USA*

[2]*Institute for Theoretical Physics, Vienna University of Technology, Vienna, Austria, EU*

[3]*Physikalisches Institut, Albert-Ludwigs-Universität Freiburg, Freiburg, Germany, EU*

(Received 8 May 2014; published 1 July 2014)

The efficient production of very-high-n, $n \sim 300$, quasi-one-dimensional (quasi-1D) strontium Rydberg atoms through three-photon excitation of extreme Stark states in the presence of a weak dc field is demonstrated using a crossed laser-atom beam geometry. Strongly polarized quasi-1D states with large permanent dipole moments $\sim 1.2n^2$ a.u. can be created in the beam at densities ($\sim 10^6$ cm^{-3}) where dipole blockade effects should become important. A further advantage of three-photon excitation is that the product F states are sensitive to the presence of external fields, allowing stray fields to be reduced to very small values. The experimental data are analyzed using quantum calculations based on a two-active-electron model together with classical trajectory Monte Carlo simulations. These allow determination of the atomic dipole moments and confirm that stray fields can be reduced to $\leqslant 25$ μV cm^{-1}.

DOI: 10.1103/PhysRevA.90.013401 PACS number(s): 32.80.Ee, 32.80.Rm, 32.60.+i

I. INTRODUCTION

Long-range interactions in many-body systems give rise to a rich variety of phenomena of fundamental importance in many areas of physics. These include creation of exotic spin and magnetic states [1], phase transitions to strongly correlated classical crystals [2,3] and supersolidity [4,5]. While a number of systems have been proposed to study such effects including ultracold polar molecules [6] and ultracold gases of atoms with large magnetic moments [7,8], Rydberg atoms offer a number of advantages because their extreme dipole moments result in interactions that can be many orders of magnitude larger than the interactions between polar molecules or atomic magnetic moments. Furthermore, the strength of Rydberg interactions can be simply controlled by varying n or (at high n) by manipulating the Rydberg state using a carefully tailored sequence of short electric field pulses [9,10]. Atomic interactions can also be controlled by optically dressing an atomic ground state with a small admixture of an excited Rydberg state [11–13].

The study of Rydberg-Rydberg interactions requires the production of two (or more) Rydberg atoms at well defined separations in well defined initial states. In the present work we examine how this might be accomplished in an atomic beam using strongly polarized quasi-one-dimensional (quasi-1D) high n, $n \sim 300$, Rydberg atoms created by exciting extreme redshifted Stark-like states in the presence of a weak dc field. The controlled production of Rydberg atoms with well defined spacings can be achieved by taking advantage of dipole blockade [14,15]. Blockade occurs when excitation of one atom inhibits subsequent excitation of its neighbors due to energy shifts associated with dipole-dipole (or van der Waals) interactions. The dipole moments of extreme Stark states are large, and simple estimates suggest that dipole-dipole interactions will give rise to energy level shifts of $\sim$13 MHz at internuclear separations of $\sim 100\mu$m that are sufficient, when using lasers with effective line widths of $\sim$10 MHz, to induce blockade. Such large blockade radii will allow creation of Rydberg atoms at well defined locations by confining excitation to localized volumes, smaller than the blockade radius, defined by tightly collimated laser and/or atom beams. This approach, however, requires high Rydberg photoexcitation rates to ensure that one (quasi-1D) Rydberg atom is created in each volume.

Quasi-1D high-n, $n \sim 300$, potassium Rydberg atoms have been created by direct single-photon excitation of "nD" states in the presence of a small applied dc field, $F_{\rm dc}$ [16,17]. (Here the notation "nD" is used to denote the zero-field state that connects adiabatically to the state excited in the field.) In weak applied fields potassium "nD" states display only a quadratic Stark effect and their polarization is very small. However, in applied fields $F_{\rm dc}$ of $\sim 0.5F_{\rm cross}$, where $F_{\rm cross} \simeq 1/(3n^5)$ is the field at which states in neighboring n-manifolds first cross, the "nD" states undergo a strong avoided crossing with the lowest-lying states in the neighboring Stark manifold (atomic units are used throughout unless otherwise noted.) As a result, the "nD" states acquire a sizable polarization and strong ℓ-mixing with the nP states allows them to be produced by single-photon excitation, although the oscillator strengths for their excitation are relatively small. This, when combined with the low laser powers available at the required UV excitation wavelengths, results in very low excitation rates. More recently, substantially higher rates for the production of quasi-1D states have been obtained through two-photon excitation of strontium "nD" states [18,19,20]. In this case, however, the "nD" states have their maximum oscillator strengths near $F_{\rm dc} = 0$, and these decrease as $F_{\rm dc}$ increases (i.e., as L-mixing increases) and the states become more polarized. Nevertheless, given the relatively large laser powers available at the required excitation wavelengths, densities of $\sim 10^5$ cm^{-3} have been achieved in a strontium atomic beam for $n \sim 300$ "nD" states having dipole moments of $\sim(1.1$–$1.2)n^2$ a.u.

In the present work we demonstrate that much higher densities of quasi-1D states can be generated by three-photon excitation of strontium "nF" states. Such states have a larger polarizability than "nD" states and even in small applied fields, $F_{\rm dc} \sim (0.2$–$0.3)F_{\rm cross}$, interact strongly with the neighboring Stark manifold. Quantum simulations indicate that the "nF" states excited in fields of $\sim 0.3F_{\rm cross}$ have sizable dipole moments, $\sim 1.2n^2$ a.u., which is verified experimentally using

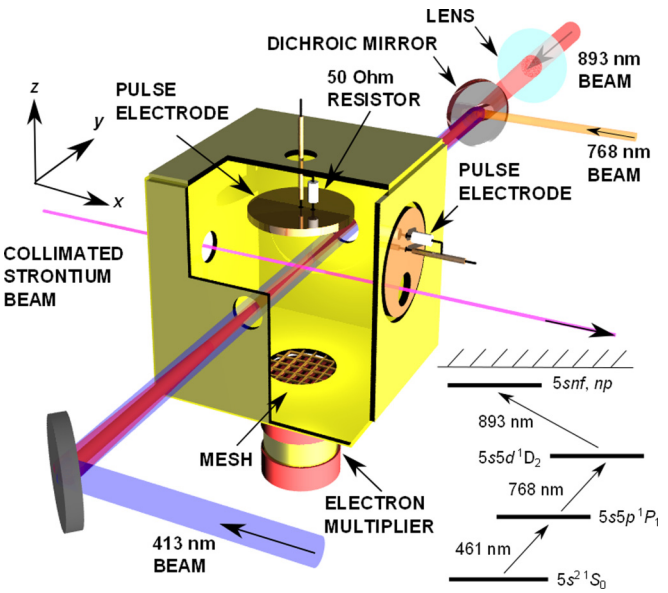

FIG. 1. (Color online) Schematic diagram of the apparatus. The inset in the lower right corner shows the three-photon excitation scheme employed.

two different methods [19]. Furthermore, the data indicate that, using 0.6-μs-long laser pulses, Rydberg atom densities greater than $\sim 1.5 \times 10^6$ cm^{-3} might be produced. Such densities, however, correspond to average interparticle separations of $\sim$90 μm, suggesting that dipole blockade effects will limit the densities that can actually be achieved. Access to this dipole-blockaded regime will enable detailed studies of the interactions between strongly coupled Rydberg atom pairs and their dependence on the coupling strength which can be varied by changing n, the atom separation, and by manipulation of the atomic state.

II. EXPERIMENTAL APPROACH

The present apparatus is shown schematically in Fig. 1. Briefly, strontium atoms contained in a tightly collimated beam are excited to the desired high-n "nF" state in the presence of a small dc field, $F_{\rm dc}$, using the crossed outputs of three lasers. The three-photon excitation scheme employed is diagramed in the inset and utilizes the $5s5p\ ^1P_1$ and $5s5d\ ^1D_2$ intermediate states and radiation at 461, 768, and 893 nm. (The decay rates associated with the $5s5d\ ^1D_2 \rightarrow 5s6p\ ^1P_1$ and $5s5p\ ^1P_1 \rightarrow 5s4d\ ^1D_2$ transitions are small and population transfer to these states is unimportant on the $\sim$1 μs time scale of the present experiments.) The radiation at 461 and 768 nm is provided by diode laser systems, that at 893 nm by a Ti:sapphire laser. The 461- and 768-nm beams are both polarized along the z axis indicated. The 893-nm beam is polarized along the x axis. When the dc field, $F_{\rm dc}$, is directed along the z (x) axis, the excited "nF" states are superpositions of $M_z = \pm 1$ ($M_x = 0, \pm 2$) levels where M_i is the magnetic quantum number relative to the corresponding orientation of the quantization axis i ($i = x,z$). The 461-nm beam propagates in the opposite direction to the other two beams to minimize Doppler effects associated with atom beam divergence resulting in an overall experimental linewidth of $\sim$5 MHz full width at half maximum (FWHM). The strontium atom beam is provided by an oven that can operate at temperatures of up to $\sim$680 °C and which can, following collimation, provide a 1-mm-diameter beam with a FWHM divergence of $\sim$4 mrad at densities approaching $\sim 10^9$ cm^{-3}. Stray fields in the experimental volume are minimized by application of small offset potentials to the electrodes that define the interaction region.

Measurements are conducted in a pulsed mode. The output of the 461-nm laser is chopped into a series of pulses of $\sim$0.6 μs duration and $\sim$20 kHz repetition frequency using an acousto-optical modulator (the other beams remain on at all times). This pulse width was selected because for shorter pulse lengths the widths of the spectral features become increasingly transform limited. The 461- and 768-nm beams are unfocused and have diameters of $\sim$3 mm. Their intensities, $\sim$10 mW cm^{-2}, were chosen to limit line shifts and broadening associated with effects such as the ac Stark shift and Autler-Townes splitting. The 893-nm beam is focused to a spot with a FWHM diameter of $\sim$200 μm, resulting in an intensity of $\sim$3 kW cm^{-2}. The frequencies of all the lasers employed here were stabilized and controlled with the aid of optical transfer cavities locked to a polarization-stabilized HeNe laser. Following excitation the polarization of the states is examined by application of a carefully tailored series of short electric field pulses that ionize a fraction of the Rydberg atoms. The probability that a Rydberg atom survives the probe pulses (or is ionized by them) is determined by selective field ionization for which purpose a slowly varying (rise time $\sim$1 μs) electric field is generated in the interaction region by applying a positive voltage ramp to the lower electrode. Product electrons are accelerated out of the experimental volume and are detected by a bell-mouthed channeltron. To allow reliable measurement of the number of Rydberg atoms initially present, the probability that a Rydberg atom was detected following any laser pulse was maintained below $\sim$0.5 to limit dead-time correction effects. To permit survival probabilities (or ionization fractions) to be determined, the number of Rydberg atoms initially created is monitored at periodic intervals during data acquisition through measurements in which no pulsed fields are applied.

The techniques used to probe the Rydberg atom polarization are described in detail elsewhere [16,19]. Briefly, in the first approach, a probe pulse of duration $T_p \sim 2.3T_n$ ($T_n = 2\pi n^3$) applied either parallel or antiparallel to the polarization axis is used to ionize a fraction of the Rydberg atoms present. For a polarized atom, the ionization fraction is sensitive to the direction in which the pulse is applied. Thus measurements of ionization fractions and their asymmetry can be mapped to the polarization of the initial state. In the second approach, the quasi-1D atoms are used as a starting point to engineer localized wave packets that travel in near-circular Bohr-like orbits [21,22]. To create such states quasi-1D atoms polarized along (say) the x axis are subject to a transverse pump field, $F_{\rm pump}$, that is suddenly applied ($T_{\rm rise} \ll T_n$) along the z axis. After one quarter of a Stark period, i.e., at $T_{\rm pump} = \pi/\omega_s$, where $\omega_s = (3/2)nF_{\rm pump}$ is the Stark precession frequency, $F_{\rm pump}$ is turned off which leaves the atom frozen in a near-circular high-L state localized near the xz plane. This state subsequently undergoes strong transient localization in azimuthal angle creating a localized wave packet that moves

TABLE I. Model potential parameters used for the TAE calculations [Eq. (2)]. The parameters are chosen to reproduce the quantum defects for high-lying singlet states.

	Strontium model potential ($\alpha_{cp} = 5.3$)			
L	α_1^L	α_2^L	α_3^L	r_c^L
0	3.008	1.000	1.073	3.000
1	3.000	0.190	0.531	2.100
2	4.200	9.735	1.873	1.000
$\geqslant 3$	4.811	4.068	1.755	0.946

in a near-circular orbit. The time evolution of this wave packet is monitored using a probe pulse similar to that employed to directly monitor the polarization of the initial state, applied either along the x or the z axis. Since the characteristics of the wave packet depend markedly on the polarization of the initial state, the observed survival probabilities provide an alternative measure of this polarization.

III. PHOTOEXCITATION IN THE ABSENCE OF DC FIELD

The measured Rydberg excitation spectra are analyzed by quantum calculations (see Ref. [18] for details) based on a two-active-electron (TAE) model. The Hamiltonian reads

$$H = \frac{p_1^2}{2} + \frac{p_2^2}{2} + V_{\ell_1}(r_1) + V_{\ell_2}(r_2) + \frac{1}{|\vec{r}_1 - \vec{r}_2|}, \qquad (1)$$

where $V_{\ell_i}(r_i)$ is an angular-momentum-dependent model potential representing the Sr^{2+} ion given by

$$V_\ell(r) = -\frac{1}{r}\left[2 + 36\exp\left(-\alpha_1^\ell r\right) + \alpha_2^\ell\, r\, \exp\left(-\alpha_3^\ell r\right)\right] - \frac{\alpha_{cp}}{2r^4}\left[1 - \exp\left[-\left(r/r_c^\ell\right)^6\right]\right]. \qquad (2)$$

Our previous studies [18,19] employed the model potential taken from Refs. [23,24] originally developed for the analysis of low-lying states and for which the quantum defects of nP and nD states with high-lying n were slightly underestimated. In the present study the parameters for the model potential are adjusted (Table I) so that the calculated energies of the high-lying ($n > 20$) singlet states agree better with the measured values [25]. For low-lying states the model potential is optimized to yield accurate values of the energies of the $5s5s$ $^1S_0$, $5s5p$ $^1P_1$, and $5s5d$ $^1D_2$ states. This allows the oscillator strengths for the three-photon excitation scheme employed here to be reliably calculated.

Figure 2(a) shows the calculated Stark energy levels for the $|M| = 1$ singlet states of strontium near $n \sim 50$. We exploit the scaling properties of Rydberg manifolds [18] to infer spectroscopic data for $n \sim 300$ from the results near $n = 50$ for which the converged numerical solution of the Schrödinger equation is still feasible. To further this comparison the results are presented in scaled units. The applied dc field, F_{dc}, is scaled to the crossing field, F_{cross}, and a scaled energy of one corresponds to the energy separation between adjacent n levels. Figure 2(a) also includes calculated ($n \sim 50$) and measured ($n \sim 306$) excitation spectra. In zero applied field a series of strong peaks is evident that corresponds to excitation of nF states, together with a series of smaller peaks that correspond to the production of nP states.

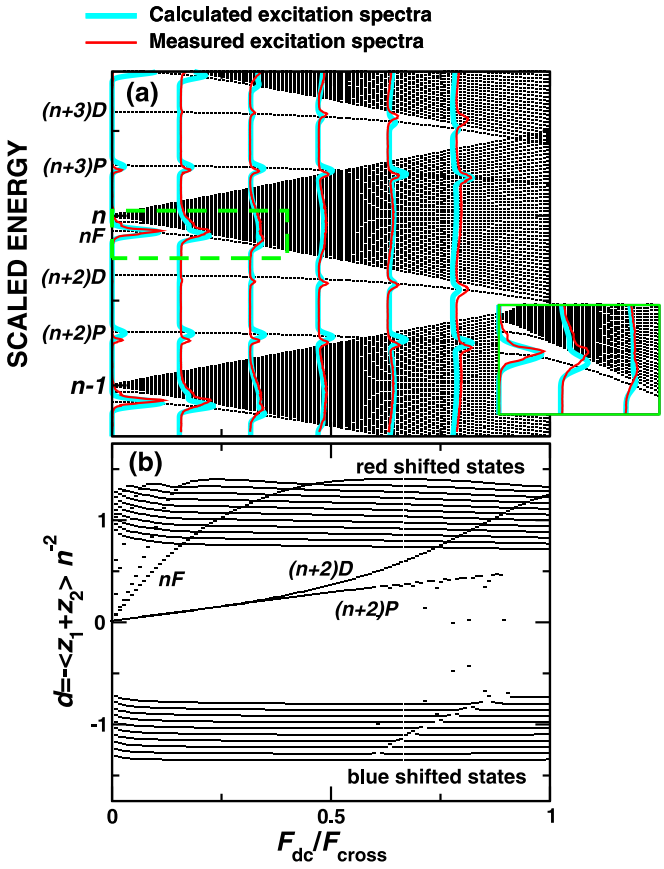

FIG. 2. (Color online) (a) Evolution of the Stark energy levels for strontium $|M| = 1$ states in the vicinity of $n = 50$ (black lines) calculated using a two-active-electron model. The thick blue (gray) lines show the calculated spectrum for excitation of "nF" states, the red (dark gray) lines show the measured excitation spectrum at $n \sim 306$. The applied dc field is normalized to the crossing field (see text). The energy axis is scaled such that a scaled energy of one corresponds to the energy separation between neighboring n and $(n-1)$ states. The inset shows an expanded view in the low-field region (indicated by the dashed square). (b) Applied field dependence of the calculated average dipole moment of several states including "nF" states.

Interestingly, the size of the "zero-field" nF features was found to be very sensitive to the presence of small stray fields. In consequence, measurements of "zero-field" spectra were used to control and to minimize the stray field in the interaction region, which is accomplished by application of small offset potentials to the electrodes surrounding the experimental volume. This approach proved superior to that used in earlier studies which was based on the measurement of Stark energy shifts which are less sensitive to external fields [26]. The attendant reduction in the stray field, and stray field inhomogeneities, allowed Rydberg series to be observed for values of n up to $n \sim 600$, significantly higher than possible previously. Since the effects of stray background fields typically become important when they approach the fields F_{cross}, at which states in neighboring manifolds first cross, this suggests that stray fields can be reduced to

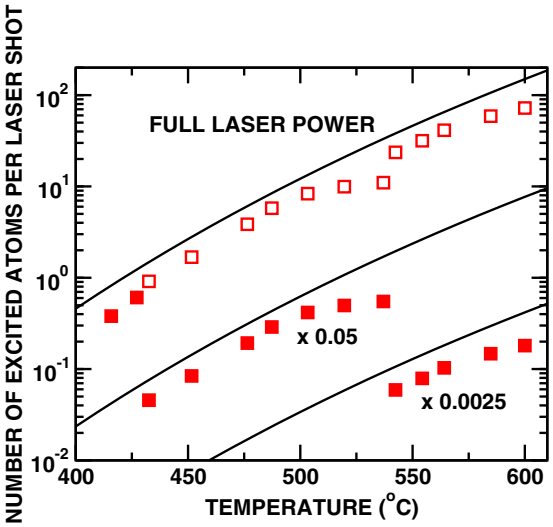

FIG. 3. (Color online) The average number of $306F$ Rydberg atoms excited during a 0.6-μs-duration laser pulse as a function of the oven temperature. The solid symbols show the results of measurements in which the production rate was limited by reducing the intensity of the 893 nm beam by the factors indicated. The open squares show the excitation probabilities expected (in the absence of dipole blockade) when using the full laser intensity. The calculated results (solid lines) employ a four-level model multiplied by the number of atoms within the interaction volume derived from the vapor pressure [27].

$\leqslant 25\ \mu\text{V cm}^{-1}$. As will be shown later, this reduction allows the free evolution of electronic wave packets over several microseconds without any significant decoherence.

The photoexcitation rates achieved using "nF" states are illustrated in Fig. 3. In these experiments a 600-ns-long 461-nm laser pulse was employed, and the probability that a Rydberg atom be created during each laser pulse determined. Since the present experimental setup does not allow the detection of more than one Rydberg atom following a laser pulse, the probability for detection of a Rydberg atom was intentionally kept below $\sim$0.5 to limit the size of the necessary dead-time corrections. This was accomplished by restricting the Rydberg atom production rate using neutral density filters inserted in the 893-nm beam. Figure 3 shows the excitation probabilities (filled squares) for $306F$ states measured in "zero-field" as a function of oven operating temperature, together with the extrapolated excitation probabilities (open squares) that might be realized when using the full laser power if blockade effects are not present. As expected, the Rydberg atom production rate increases steadily with oven operating temperature. For temperatures of 600 °C a production rate of about 100 Rydberg atoms per laser shot is expected at full laser power which, when allowance is made for the motion of atoms in the beam during the 600-ns laser pulse, corresponds to a Rydberg atom density of $\sim 5 \times 10^6\ \text{cm}^{-3}$. (This is substantially higher than that achieved in zero field for two-photon excitation of nD states [18], in part due to the high output powers available at 893 nm from the Ti:sapphire laser.) The measured excitation probability is consistent with the probability calculated (solid lines) using a four-level model involving the $5s^2\ ^1S_0$, $5s5p\ ^1P_1$, $5s5d\ ^1D_2$, and $5s306f\ ^1F_3$ states driven by three laser pulses. The dipole transitions between low-lying states are extracted directly from the TAE calculation while the transition between $5s5d$ and $5s306f$ is extrapolated from the values obtained for $n \sim 50$. The excitation probability (after 600 ns) is averaged over a randomly distributed range of laser detunings to mimic the Doppler broadening and is multiplied by the temperature-dependent number of atoms in the interaction volume derived from the vapor pressure [27]. The temperature-dependent excitation rates inferred from the experimental measurements match well the theoretical predictions, which also neglect possible blockade. (The apparent "steps" in the Rydberg production rate evident upon insertion of the neutral density filters are attributed to uncertainties in the dead-time correction.) The good agreement between theory and experiment indicates that the number of excited atoms is proportional to the 893 nm laser intensity and, therefore, that high Rydberg atom densities can indeed be realized at full laser power.

IV. EXCITATION OF QUASI-1D STATES IN A DC FIELD

One motivation of the present work is to access the regime in which strong dipole-dipole interactions become important. The strength of such interactions can be controlled by the creation of quasi-1D states having different dipole moments. This can be achieved by photoexcitation in the presence of a dc field. Whereas for $F_{\text{dc}} = 0$ the selection rules allow the excitation of nF and nP states, the L-mixing induced by the presence of a dc field allows production of polarized states. With increasing F_{dc} the "nF" states undergo a strong avoided crossing with the most strongly redshifted states in the neighboring Stark manifold and thus rapidly assume the character of these strongly polarized quasi-1D states. This growth in polarization is also evident in the calculated expectation values of the dipole moment $d = -\langle z_1 + z_2 \rangle$ [Fig. 2(b)]. The dipole moment grows linearly at small F_{dc} and reaches its near maximum value of $\sim 1.2n^2$ at values of $F_{\text{dc}} \geqslant 0.25 F_{\text{cross}}$. On the other hand, the "nP" states are only weakly coupled to their adjacent Stark states resulting in very little change in their energy and in small polarizations. The different response of the nF and nP states to the field is also observable in the sizes of their associated spectral features. As F_{dc} increases the "nP" features remain sizable whereas, as shown in more detail in the inset, the size of the "nF" features decreases markedly, a consequence of the strong mixing with neighboring (higher-L) Stark states which reduces their $L = 3$ character. Nonetheless, even for values of $F_{\text{dc}} \sim 0.3 F_{\text{cross}}$ (where the predicted polarization is large), the size of the "nF" features is only reduced by $\sim$60%, and significant excitation probability remains indicating that densities as high as $\sim 1.5 \times 10^6\ \text{cm}^{-3}$ should (neglecting blockade) be achievable. This corresponds to an average interparticle separation of $\sim$90 μm which is smaller than the separation at which blockade effects should become important. In the absence of blockade, even higher Rydberg densities might be achieved by modifying the apparatus so as to position the 893 nm focusing lens within the vacuum system and thereby create a tighter focal spot. Inspection of Fig. 2 also shows that for values of $F_{\text{dc}} \geqslant 0.8 F_{\text{cross}}$ sizable production

rates for "nD" states can be achieved that are comparable to those for "nF" states at $F_{dc} \sim 0.25 F_{cross}$.

V. PROBING THE DIPOLE MOMENT

In this section the dipole moment $d = -\langle z_1 + z_2 \rangle$ of the excited strontium "nF" Rydberg states is analyzed by two probing methods [19]. The probing techniques monitor the ionization induced by probe pulses. The dipole moment is determined by comparing experimental data to the results of simulations undertaken utilizing classical trajectory Monte Carlo (CTMC) techniques. Since the highly excited Rydberg electron barely interacts with the core electrons, the CTMC simulations are performed using a single-active-electron (SAE) model (see Ref. [19] for more details). In these simulations, the well polarized "nF" states, perturbed by the dc field, are approximated by an ensemble of parabolic states [16] whose average dipole moments are taken from the quantum TAE calculations. For comparison, the ionization of other states, such as the "nP" and "nD" states, is also considered. Because of their weak L-mixing, these states do not have obvious classical counterparts and are approximated by an ensemble for which not only the average dipole moment but also the dipole moment distribution is derived from quantum calculations.

A. Ionization by a field step

The first probing technique employs a probe field in the form of a field step,

$$F = \begin{cases} F_{step} & 0 \leqslant t \leqslant T_p, \\ 0 & \text{elsewhere}, \end{cases} \tag{3}$$

where $T_p \sim 2.3 T_n$ is the pulse duration. The asymmetry in the ionization fractions observed, when the probe field is applied parallel and antiparallel to the polarization axis, can be used as a measure of the polarization of the target state [19]. Results for the ionization of "$306F$" states by the probe field are presented in Fig. 4 for several values of applied field, F_{dc}. Note that, once the "$306F$" state merges with the Stark manifold, the laser is tuned to the lower edge of the manifold. Pronounced asymmetries in the ionization probabilities are observed that grow as F_{dc} is increased, consistent with the predicted increase in polarization of the excited states (see Fig. 2). The data in Fig. 4 show that the size of the field step required to ionize states whose dipole moments are oriented anti-parallel to F_{step} depends markedly on F_{dc}. In contrast, the ionization of states whose dipole moments are oriented parallel to F_{step} is relatively insensitive to the size of F_{dc}. This results because in the latter case the state is oriented towards the saddle point in the electron potential created by application of F_{step} allowing the electron easy escape. This is not the case when F_{step} is reversed. The electron must now cross the atom to escape and this is hindered by strong scattering from the core ion. Figure 4 also includes the results of CTMC simulations which agree well with the measured data for all values of F_{dc}. In particular, at $F_{dc} = 0.4 F_{cross}$, the theoretical predictions, which are derived using the calculated dipole moment of $\sim 1.2 n^2$ a.u., are in good agreement with the experimental results indicating that the "nF" states are indeed strongly polarized.

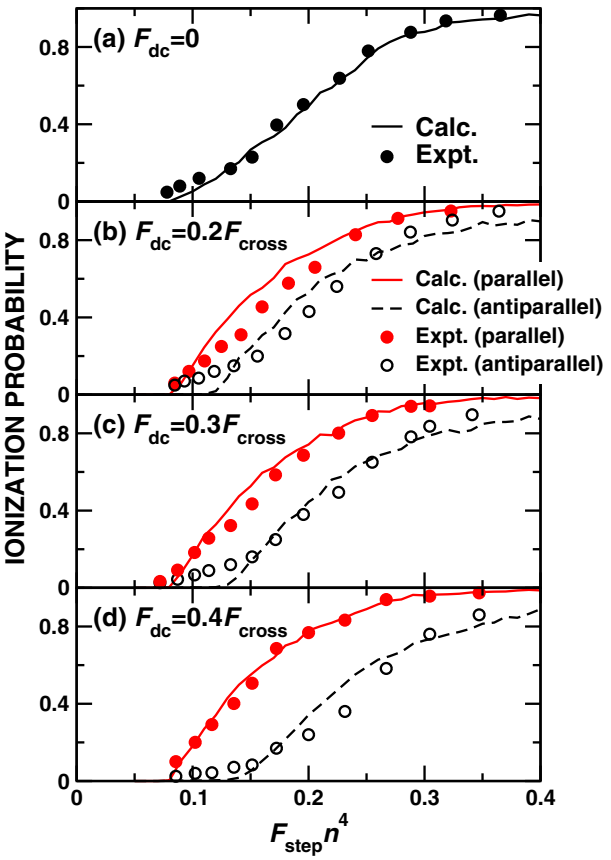

FIG. 4. (Color online) Measured ionization probabilities for "$306F$" states excited in the dc fields indicated as a function of the scaled amplitude of a probe field, $F_{step}n^4$, of 10 ns duration, $T_p \sim 2.3 T_n$. Solid (open) circles denote data points recorded with the probe field applied parallel (antiparallel) to the dc electric field F_{dc}. The solid (dashed) lines show the ionization probabilities calculated with the probe field parallel (anti-parallel) to F_{dc}. As the initial state, the CTMC calculations employ (a) a microcanonical ensemble restricted to $\ell = 1$ and $m = 1$ and (b)–(d) an ensemble of 13 parabolic states with an average k of (b) $k = 166$, (c) $k = 212$, and (d) $k = 244$.

As evident from Fig. 2, at intermediate values of $F_{dc} \sim 0.4 F_{cross}$ the excitation spectrum contains relatively broad features associated with excitation of states in the Stark manifold. This allows a measure of control to be exerted over the polarization and orientation of the product states by tuning the laser to different points in the manifold. Excitation of extreme redshifted (blueshifted) Stark states will lead to production of strongly polarized quasi-1D "downhill" ("uphill") states whereas excitation near the center of the manifold should result in the formation of states having little polarization. This is demonstrated in Figs. 5(a)–5(c) which show asymmetries measured with the laser tuned to the positions indicated in the inset. As expected, a large asymmetry is observed with the laser red-detuned to the lower edge of the manifold. Little asymmetry is evident with the laser tuned near the center of the manifold, consistent with the creation of states having only very small dipole moments. When the laser is blue-detuned towards the upper edge of the manifold an asymmetry in the survival probabilities again appears but in the opposite sense to that seen for red detuning. The magnitude in the asymmetry

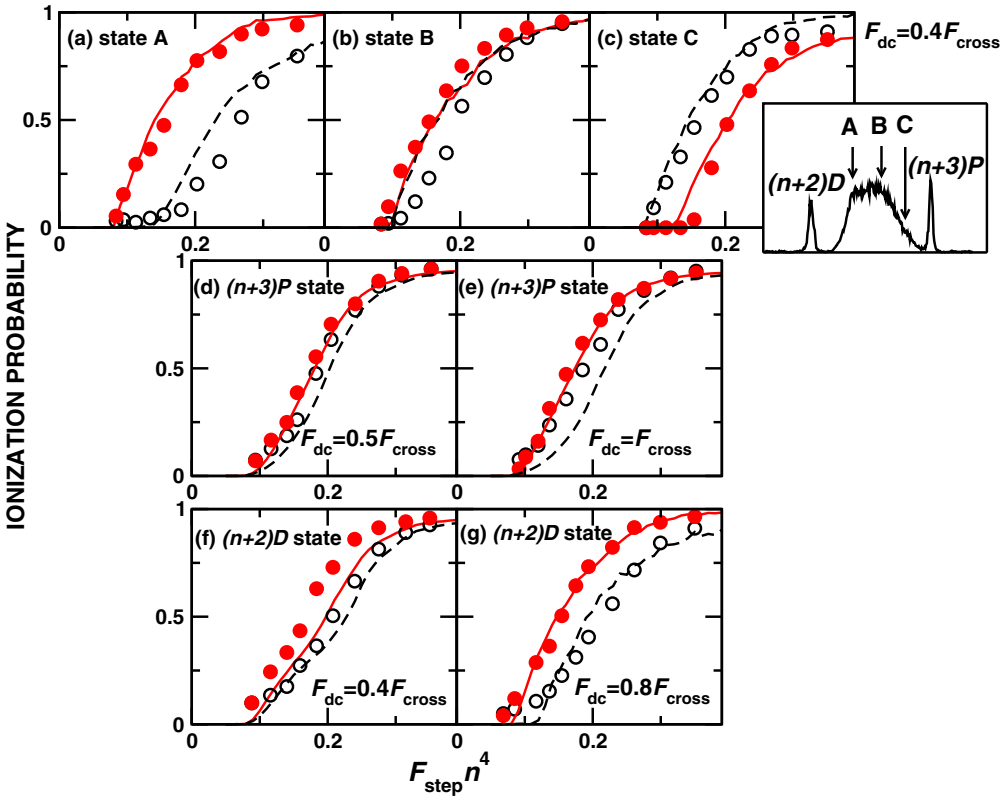

FIG. 5. (Color online) (a)–(c) Measured ionization probabilities for $n \sim 306$ states excited in a dc field $F_{dc} \sim 0.4F_{cross}$ with the laser tuned to the points (A–C) indicated in the spectrum in the inset as a function of the scaled amplitude of a 10 ns probe field, F_{step}. Solid (open) circles denote data points recorded with the probe field applied parallel (anti-parallel) to F_{dc}. Measured ionization probabilities [(d) and (e)] for "309P" states and [(f) and (g)] for "308D" states excited in the dc fields F_{dc} indicated. The CTMC simulations employ, as the initial state, an ensemble of 13 parabolic states with an average k of (a) $k = 244$, (b) $k = 0$, and (c) $k = -195$ and (d)–(g) a distribution derived from the quantum TAE calculations [19]. The probe field amplitude is indicated in scaled units, $F_{step}n^4$.

is somewhat lower than that seen for the corresponding red detuning from the center of the manifold. This is because the most blue-shifted states have the smallest oscillator strengths and photoexcitation emphasizes the production of the less polarized states whereas for the redshifted states the oscillator strengths peak at the most polarized states.

Figures 5(d)–5(g) show the asymmetry measured for the "309P" and "308D" states. The "309P" state is only weakly polarized for all values of $F_{dc} < F_{cross}$. Since the "309P" state overlaps the Stark states that have the opposite polarization, the experimental data are influenced by this admixture which will reduce the measured asymmetry. The theoretical predictions, however, are for a pure "nP" state and do not include this admixture of Stark states. Therefore, a small asymmetry is predicted. For the "308D" state strong interactions with the nearby redshifted Stark states are expected beyond $F_{dc} \sim 0.8F_{cross}$. Sizable asymmetries are again seen and agree reasonably well with the calculations, in particular at $F_{dc} = 0.8F_{cross}$. We note that the initial ensembles used in the calculations are designed to represent the states excited in the two limiting cases of either weak or strong L-mixing. Small deviations from the measured results are therefore seen for states featuring moderate L-mixing such as in Fig. 5(f) (see [19] for a more detailed discussion). The observed asymmetries are somewhat smaller than those observed following two-photon excitation of ($M = 0$) "nD" states in similar fields and those obtained by three-photon excitation of "nF" states at lower applied fields. However, the "nD" production rates achieved are much larger than for two-photon excitation.

B. Production of near-circular states

The polarization of the initial quasi-1D states can also be inferred through their conversion into near-circular wave packets by a pump pulse [19]. A well polarized state can be transformed into a near-circular wave packet whose orbital plane is defined by the polarization axis and the pump field orientation. A less polarized state, i.e., one whose dipole moment not perfectly aligned with F_{dc} but is rather distributed in space, is transformed into a circular wave packet whose plane of orbit is not well defined. Such a difference affects the time development of the expectation values $\langle x(t)\rangle$ and $\langle z(t)\rangle$ which can be monitored using a probe field. Here "309F" states created in a dc field $F_{dc} \sim 0.3F_{cross}$ along the x axis were subject to a 5 mV cm^{-1} 80-ns-long transverse pump pulse applied along the z axis. The subsequent evolution of the resulting wave packet was monitored by application of a 6-ns-long field step of amplitude $F_{step} \sim 100$ mV cm^{-1} along either the x or z axis. The resulting measured survival probabilities mirror the expectation values $\langle x(t)\rangle$ and $\langle z(t)\rangle$ and are shown in Fig. 6 as a function of the time delay, t_d, between the end of the pump pulse and application of F_{step} together with

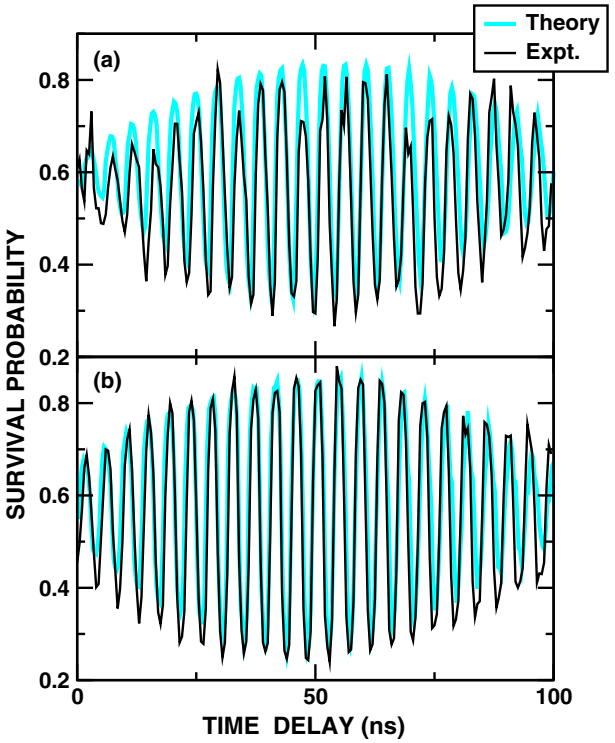

FIG. 6. (Color online) Survival probabilities measured (black lines) for "309F" states produced in a field $F_{dc} \sim 0.3F_{cross}$ and subject to a 5 mV cm^{-1} 80-ns-long pump pulse, F_{pump}, as a function of the time delay between the end of F_{pump} and the application of a 6-ns-long probe pulse $F_{step} \sim 100$ mV cm^{-1}. The blue (gray) lines show the result of CTMC simulations in which the initial state is represented by an ensemble of 13 parabolic states with an average $k \simeq 224$ and $m = 2$. In (a) the probe pulse is parallel to F_{dc}, in (b) parallel to F_{pump}.

the results of theoretical simulations. The buildup of strong oscillations in survival probability, i.e., in $\langle x(t)\rangle$ and $\langle z(t)\rangle$, is seen [21] that results from strong transient localization of the wave packet. The near-equal size of the oscillation amplitudes when probing along both the x and z axes indicates creation of a circular wave packet that is confined almost within the xz plane, implying that the initial state is near maximally polarized. Comparison between theory and experiment again points to the creation of states with dipole moments of $\sim 1.2n^2$.

VI. DECOHERENCE-FREE EVOLUTION OF BOHR WAVE PACKETS

The strong sensitivity of F states to external fields allows stray fields within the interaction volume to be reduced to very low values. Such a low-field environment provides the opportunity to observe the nearly decoherence-free evolution of Rydberg wave packets over extended periods of time. This is demonstrated by monitoring the collapse and revival of transiently localized near-circular "Bohr-like" wave packets [28]. Since the wave packet comprises a coherent superposition of different n states, the distribution of the n-dependent angular frequencies, $\omega_n = E_n - E_{n-1}$, leads to dephasing and delocalization of the wave packet, which results in a marked reduction in the amplitude of the quantum beats (see Fig. 6).

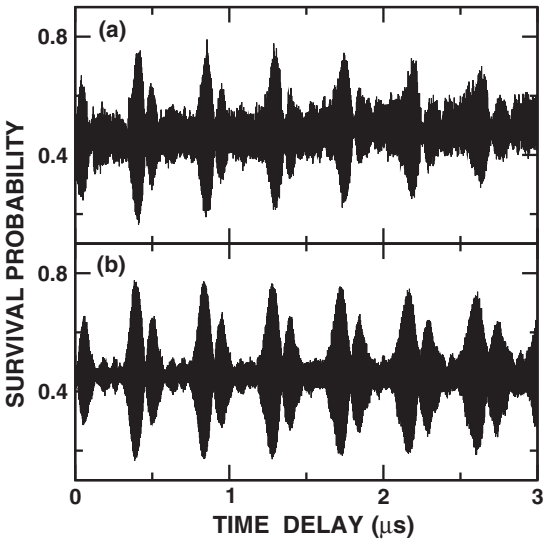

FIG. 7. (a) Measured and (b) calculated survival probabilities for "306F" states as a function of the time delay, t_d, between turn-off of the pump field F_{pump} and application of the probe pulse $F_{step} \sim 120$ mV cm^{-1} in the z direction. Shown is the envelope of the unresolved fast quantum beats with period $T_n \simeq 4.3$ ns (see Fig. 6).

However, when the number of n states involved is small, the different components can move back into phase (modulus 2π) recreating a localized wave packet and a revival in the quantum beat amplitude. The time between successive revivals is given approximately by [29]

$$T_R = \frac{2\pi}{\omega_n - \omega_{n+1}} \simeq \frac{2\pi n^4}{3}. \quad (4)$$

However, inhomogeneous line broadening such as that induced by stray fields or electrical noise can smear out the discreteness of the frequency spectrum, ω_n, leading to the suppression of the revivals. Thus, the amplitude of the revivals provides a measure of the strength of the interaction with the environment, i.e., of irreversible dephasing or decoherence. The revivals of the near circular wave packet generated from the "306F" state created in $F_{dc} \sim 0.3F_{cross}$ are displayed in Fig. 7(a). The fast quantum beats (visible in Fig. 6) have the frequency of the classical orbital motion, $2\pi n^3 \simeq 4.3$ ns. Figure 7 shows the envelope of the fast beats. A pronounced series of revivals is observed at intervals of $T_R \simeq 400$ ns and extends for several microseconds. While similar quantum revivals have been seen previously with potassium "nD" states [28], the rate of decay of their amplitude was much faster than observed here. This is, at first glance, counterintuitive given the strong coupling of strontium "nF" states to the environment. However, the pump field F_{pump} rapidly transforms the low-L states into high-L wave packets for which the coupling to the environment is rather insensitive to the exact value of L and is determined primarily by the size of the stray fields. Therefore, by better suppressing stray fields and stray field inhomogeneities in the experimental volume the coherence time is greatly extended. Calculated survival probabilities are included in Fig. 7(b). The calculations employ the CTMC method with an initial ensemble whose energy spectrum is quantized so that quantum revivals can be well reproduced (see Ref. [28] for more details).

A slow decay in the amplitude of the revivals is evident even in the "coherent" evolution of the calculated beat pattern. This results because the rate of dephasing, $\omega_n - \omega_{n+1}$, has a weak n dependence and, therefore, the rephasing of all the n states is not perfectly simultaneous. This small mismatch leads to a reduction in the revival amplitude even for coherent evolution. The decay rate of the measured revival amplitudes is very similar to that seen in the calculations which assume a decoherence-free environment. The data thus demonstrate that remarkably long coherence times of several microseconds can be achieved in mesoscopic systems such as high-n Rydberg atoms through the effective reduction of stray fields.

VII. FUTURE DIRECTIONS

The present study shows that strongly-polarized strontium "306F" Rydberg atoms with dipole moments of $\sim 1.2n^2$ a.u. can be efficiently produced in a beam through three-photon excitation in small dc fields, $F_{\rm dc} \sim (0.2\text{–}0.3)F_{\rm cross}$, with densities sufficient that interatomic Rydberg-Rydberg interactions should become important. The dipolar Rydberg-pair interaction near $n \sim 300$ is estimated to result in an energy shift of $\sim$13 MHz at an interatomic separation of 100 μm while the van der Waals interaction for a pair of unpolarized "306F" states (at the same separation) corresponds to a shift of $\sim$4.7 MHz. Three-photon excitation promises to extend Rydberg atom densities in the beam well into the blockade regime as well as providing a means to decrease stray fields within the interaction volume and thereby create a decoherence-free environment. Dipole-dipole interactions will permit the creation of Rydberg atom pairs at well defined separations through use of two localized excitation regions defined using tightly collimated atom beams and/or strongly focused laser beams. If the excitation volumes are small with linear dimensions $\leqslant$100 μm, and are sufficiently well separated, excitation of two (and only two) Rydberg atoms will occur, one in each locally blockaded region. Furthermore, if the two atoms are well separated they will initially only interact weakly. Their mutual interaction can then be increased by using one (or more) short electric field pulses to excite them to higher n levels [9,10], the degree of coupling being determined by the final target state. This will result in a transition from a weakly to a strongly interacting atom pair. Since each atom is subject to the same pulse sequence (which typically takes a time $<T_n$), excitation will lead to the quasi-sudden creation of a two-electron wave packet. Detailed analysis of its subsequent evolution can then be undertaken using further probe fields, providing a new avenue to study strongly coupled Rydberg systems. Questions of interest focus on the dynamics of energy interchange and their dependence on the degree of coupling, which can be further controlled by varying the orientation of the product states, for example, by creating dipole pairs that are aligned either side by side or end to end. Excitation to Rydberg states whose size is comparable to the interatomic spacing will lead to formation of a transient Rydberg "molecule" whose stability against autoionization is governed by electron-electron scattering. Of particular interest are long-lived configurations where, due to their correlated motions, the electrons remain far apart. Such states, which are not accessible by direct photoexcitation, provide an opportunity to create a correlated phase-locked Rydberg-pair wave packet. Extension to the use of three (or more) collinearly arranged excitation volumes promises further opportunities to explore energy interchange, to observe formation of strongly-correlated polyatomic Rydberg systems, and to examine differences in behavior between the center and outer atoms.

ACKNOWLEDGMENTS

Research was supported by the NSF under Grant No. 1301773, by the Robert A. Welch Foundation under Grant No. C-0734, by the FWF (Austria) under Grant No. P23359-N16, and by SFB-NextLite. The Vienna Scientific Cluster was used for the calculations.

[1] I. Lesanovsky, Phys. Rev. Lett. **106**, 025301 (2011).
[2] G. Pupillo, A. Micheli, M. Boninsegni, I. Lesanovsky, and P. Zoller, Phys. Rev. Lett. **104**, 223002 (2010).
[3] R. M. W. van Bijnen, S. Smit, K. A. H. van Leeuwen, E. J. D. Vredenbregt, and S. J. J. M. F. Kokkelmans, J. Phys. B: At. Mol. Opt. Phys. **44**, 184008 (2011).
[4] F. Cinti, P. Jain, M. Boninsegni, A. Micheli, P. Zoller, and G. Pupillo, Phys. Rev. Lett. **105**, 135301 (2010).
[5] M. Boninsegni and N. V. Prokof'ev, Rev. Mod. Phys. **84**, 759 (2012).
[6] L. D. Carr, D. DeMille, R. V. Krems, and J. Ye, New J. Phys. **11**, 055049 (2009).
[7] A. Griesmaier, J. Werner, S. Hensler, J. Stuhler, and T. Pfau, Phys. Rev. Lett. **94**, 160401 (2005).
[8] M. Lu, S. H. Youn, and B. L. Lev, Phys. Rev. Lett. **104**, 063001 (2010).
[9] F. B. Dunning, J. J. Mestayer, C. O. Reinhold, S. Yoshida, and J. Burgdörfer, J. Phys. B **42**, 022001 (2009).
[10] F. B. Dunning, C. O. Reinhold, S. Yoshida, and J. Burgdörfer, Am. J. Phys. **78**, 796 (2010).
[11] J. Honer, H. Weimer, T. Pfau, and H. P. Büchler, Phys. Rev. Lett. **105**, 160404 (2010).
[12] J. E. Johnson and S. L. Rolston, Phys. Rev. A **82**, 033412 (2010).
[13] K. Singer, J. Stanojevic, M. Weidemuller, and R. Cote, J. Phys. B **38**, S295 (2005).
[14] D. Comparat and P. Pillet, J. Opt. Soc. Am. B **27**, A208 (2010).
[15] E. Urban, T. A. Johnson, T. Henage, L. Isenhower, D. D. Yavuz, T. G. Walker, and M. Saffman, Nat. Phys. **5**, 110 (2009).
[16] C. L. Stokely, J. C. Lancaster, F. B. Dunning, D. G. Arbó, C. O. Reinhold, and J. Burgdörfer, Phys. Rev. A **67**, 013403 (2003).
[17] W. Zhao, J. C. Lancaster, F. B. Dunning, C. O. Reinhold, and J. Burgdörfer, Phys. Rev. A **69**, 041401 (2004).
[18] S. Ye, X. Zhang, T. C. Killian, F. B. Dunning, M. Hiller, S. Yoshida, S. Nagele, and J. Burgdörfer, Phys. Rev. A **88**, 043430 (2013).

[19] M. Hiller, S. Yoshida, J. Burgdörfer, S. Ye, X. Zhang, and F. B. Dunning, Phys. Rev. A **89**, 023426 (2014).
[20] J. Millen, G. Lochead, G. R. Corbett, R. M. Potvliege, and M. P. A. Jones, J. Phys. B **44**, 184001 (2011).
[21] J. J. Mestayer, B. Wyker, J. C. Lancaster, F. B. Dunning, C. O. Reinhold, S. Yoshida, and J. Burgdörfer, Phys. Rev. Lett. **100**, 243004 (2008).
[22] J. J. Mestayer, B. Wyker, F. B. Dunning, S. Yoshida, C. O. Reinhold, and J. Burgdörfer, Phys. Rev. A **79**, 033417 (2009).
[23] M. Aymar, C. H. Greene, and E. Luc-Koenig, Rev. Mod. Phys. **68**, 1015 (1996).
[24] E. Luc-Koenig, M. Aymar, J.-M. Lecomte, and A. Lyras, J. Phys. B **31**, 727 (1998).
[25] J. E. Sansonetti and G. Nave, J. Phys. Chem. Ref. Data **39**, 033103 (2010).
[26] M. T. Frey, X. Ling, B. G. Lindsay, K. A. Smith, and F. B. Dunning, Rev. Sci. Instrum. **64**, 3649 (1993).
[27] G. D. Maria and V. Piacente, J. Chem. Therm. **6**, 1 (1974).
[28] C. O. Reinhold, S. Yoshida, J. Burgdorfer, B. Wyker, J. J. Mestayer, and F. B. Dunning, J. Phys. B **42**, 091003 (2009).
[29] Z. D. Gaeta and C. R. Stroud, Jr., Phys. Rev. A **42**, 6308 (1990).